The Journal of Supercritical Fluids 217 (2025) 106458

Contents lists available at ScienceDirect

The Journal of Supercritical Fluids

journal homepage: www.elsevier.com/locate/supflu

# Surface wettability of lignin materials from supercritical water hydrolysis of wood

Vesna Leontijevic [a], Tijana Fechter [a], Danilo Cantero [a], Philip Jaeger [b], Maria José Cocero [a,*]

[a] BioEcoUva, Institute, PressTech Group, Chemical Engineering & Environmental Technology Department University of Valladolid, Prado de la Magdalena s/n, Valladolid 47011, Spain
[b] Institute of Subsurface Energy Systems, Clausthal University of Technology, Agricola Str. 10, Clausthal-Zellerfeld 38678, Germany

## HIGHLIGHTS

- SCWH enables control of cellulose content allowing for tailored wettability.
- Significant impact of material composition and processing on wettability and surface energy.
- Materials with higher surface energy exhibit better wettability.
- Slight increase in CA is observed with increasing pressure.

## GRAPHICAL ABSTRACT

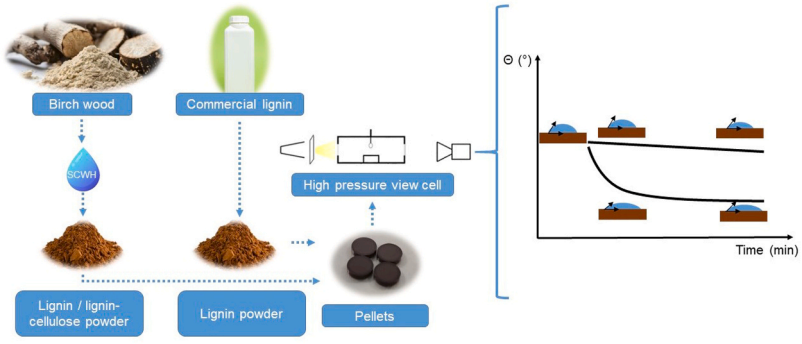


## ARTICLE INFO

*Keywords:*
Cellulose
Composites
Surface roughness
Surface energy
Pressure

## ABSTRACT

To meet the demands of the evolving circular economy, there is a growing need for renewable resources as base materials for innovative, easily recyclable products. Lignin, the second most abundant biopolymer, has emerged as a promising source of aromatics and reinforcing agent in polymer composites. For the successful manufacturing of homogeneous composite materials, good bonding between the coexisting phases is essential to prevent the formation of voids and agglomerates. Therefore, understanding the surface properties of these materials is crucial for designing optimal composite compounds. In this study, the wettability of lignin-cellulose composites and lignin samples obtained through supercritical water hydrolysis (SCWH) of birch wood is investigated. The contact angle (CA) technique, specifically the sessile drop method, was employed to assess and compare the wettability of SCWH lignin with commercially available lignin and raw birch wood. The results provide insights into their surface energy, adhesion, and hydrophilic or hydrophobic characteristics under processing conditions. All samples exhibited hydrophilicity, with an initial CA approximately 40 °, except for raw birch wood, which had a higher initial CA of ~ 64°. Notably, when lignin is accompanied by significant amounts of cellulose, different trends in CA changes over time were observed. The influence of pressure on the CA between water and these polymers was also analyzed, but no significant impact was detected. This research advances the development of lignin-based materials with tailored surface properties for various industrial applications.

* Corresponding author.
*E-mail address:* mariajose.cocero.alonso@uva.es (M.J. Cocero).

https://doi.org/10.1016/j.supflu.2024.106458
Received 5 September 2024; Received in revised form 17 October 2024; Accepted 11 November 2024
Available online 13 November 2024

## 1. Introduction

As the circular economy continues to evolve, the demand for renewable resources as foundational substances for innovative, recyclable materials is escalating. Within this framework, lignin is increasingly recognized as a valuable source of aromatics and a vital reinforcing material for polymer composites. Lignin, the second most abundant biopolymer, is the focus of growing research aimed at transforming it into a key source of aromatics, which are currently derived from petroleum [1]. New materials based on polymer-lignin composites, utilizing lignin as a reinforcing agent, are also emerging [2]. Further, a beneficial synergistic effect of lignin and cellulose mixtures used in different applications (wood adhesives, carbon fiber, nanofibers, thermoplastics) has been demonstrated [3]. On the other hand, to produce a homogeneous composite material, the polymer matrix and any reinforcing materials (such as fibers or fillers) should be chemically and physically compatible to ensure strong interfacial bonding. At the same time, the reinforcement materials have to be uniformly dispersed within the polymer matrix to avoid agglomerates, which can weaken the composite and create stress concentrations [4,5]. To select suitable composite compounds, their surface energies need to be aligned in order to reach optimal composite properties [6,7]. The surface energy of solid materials is related to their wetting behavior [8]. The wettability refers to the degree to which a liquid drop will spread over the solid surface surrounded by another fluid (liquid or gas). In case of complete wettability, the liquid will spread over the entire surface spontaneously. While wetting behavior is a universal phenomenon, it can vary based on the chemical nature of both the solid and liquid phases [9]. When the applied liquid is water, the commonly used terms to explain the wetting behavior are hydrophilicity and hydrophobicity. Hydrophilic and hydrophobic materials play crucial roles in a wide range of applications due to their distinctive interactions with water. The unique properties of hydrophilic and hydrophobic materials, enable innovative solutions across diverse sectors, enhancing functionality and performance. Hydrophilic materials are essential in industries where favorable water interaction is required, while hydrophobic materials play a crucial role in creating water-repellent surfaces, offering advantages across various industrial applications.

For the direct measurement of surface wettability, the contact angle (CA) is commonly detected optically. Therefore, the so-called sessile drop method, a versatile and relatively simple technique is frequently used [10]. The CA is the angle formed at the interface where a liquid droplet meets a solid surface. It is measured through the liquid, between the solid surface and the tangent line to the liquid droplet at the contact point. The concept of CA and wettability was introduced in 1805 by Thomas Young [11]. This technique provides valuable insights into surface energy, adhesion, and the hydrophobic or hydrophilic nature of materials. The materials that are targeted at in this work originate from natural waste that undergoes a supercritical water treatment.

Supercritical water hydrolysis is a clean technology that offers a rapid and efficient method for treating wood materials in absence of any additives or further reactants [12]. This process facilitates the dissolution and hydrolysis of cellulose in less than a second, significantly reducing processing time. Additionally, it enables the hydrolysis of the lignin-cellulose complex found in wood, aiding in the effective fractionation of its different polymers. The use of a Sudden Expansion Reactor in this technology further enhances its efficiency by rapidly cooling the reacting materials, resulting in the precipitation of unique lignin and cellulose composites [13]. Unlike conventional methods, this approach does not involve solvent dissolution or bleaching. Moreover, the native lignin structure is preserved to a significant extent, producing distinct precipitates with the potential for innovative applications [13,14].

The primary objective of this study is to evaluate the surface wettability and the related surface energies of lignin-cellulose composites produced via supercritical water hydrolysis (SCWH) and compare their properties to lignins obtained through different extraction methods, including sulfonated kraft lignin (SKL) and Indulin. By examining the surface properties, particularly through contact angle measurements, this study aims to provide critical insights into the interaction between water and these lignin-based materials. Furthermore, contact angle measurements offer a quantitative assessment of the surface energy revealing the underlying mechanisms that govern the hydrophilic or hydrophobic nature of these materials. These insights are crucial for optimizing the design of lignin-based composites in terms of compatibility of the matrix and the filler [6], and in general for functionalizing surfaces for various industrial applications. Furthermore, an additional objective is to investigate the influence of pressure on the contact angle (CA) between water and polymer surfaces. Since composite manufacturing often involves elevated pressures, this study seeks to determine whether pressure affects the surface wettability and, consequently, the performance of the final composite materials.

**Table 1**
Supercritical water hydrolysis reactions conditions for two supercritical water lignin samples (SCWL).

| Sample | Reaction time | Reaction temperature | Reaction pressure |
|---|---|---|---|
| SCWL1 | 0.34 s | 377 ± 10 °C | 284 ± 2 bar |
| SCWL2 | 1.16 s | 390 ± 2 °C | 254 ± 3 bar |

## 2. Materials and methods

### 2.1. Materials

Five different lignin samples were utilized in this study. Sulfonated kraft lignin (SKL) and commercial kraft lignin (Indulin) were sourced from Sigma Aldrich (Darmstadt, Germany) and Ingevity (formerly Mead Westvaco, North Charleston, South Carolina, USA), respectively. The third and fourth samples were obtained through SCWH of birch wood and are referred to as supercritical water lignin (SCWL). The distinction between the two SCWL lies in their cellulose content. In addition, raw birch wood was included as a fifth sample. Birch wood was provided by RISE Research Institutes of Sweden (Stockholm, Sweden). Diiodomethane, a nonpolar compound used to estimate the surface energy (SE) of the lignin-rich material, was purchased from Fisher Scientific (Bleiswijk, Netherlands). The nitrogen was purchased from Linde (Valladolid, Spain) at a purity of 5.0 (>99.999 %v).

### 2.2. Supercritical water hydrolysis of birch wood and SCWL characterization

The SCW treatment of wood primarily hydrolyzes the carbohydrates (cellulose and hemicellulose). The solid products after SCW treatment are composed mainly of lignin and cellulose based carbohydrates. Detailed experimental procedures of supercritical water hydrolysis can be found in [13]. The 2 SCWL used in this study were obtained using conditions given in Table 1.

The chemical composition (cellulose, hemicellulose, and lignin) of birch wood and the composition of SCWL were analyzed following procedures implemented by the National Renewable Energy Laboratories [15].

### 2.3. Preparation and characterization of pellets

Prior to measuring the contact angle, the samples were converted into pellets using the following technique: Approximately 0.4 g of each sample was placed in a mold with a 13 mm diameter and height of 19 mm and subjected to a hydraulic press with an applied pressure of around 7.4 Mt. The resulting pellet had a thickness of approximately 4 mm.

**Table 2**
Chemical composition of the birch wood and two supercritical water lignin samples (SCWL).

| Component | Amount (% w/w dry basis) | | |
|---|---|---|---|
| | Birchwood | SCWL1 | SCWL2 |
| Acid insoluble lignin | 13.2 ± 0.3 | 41.6 ± 2.1 | 93.8 ± 3.6 |
| Acid soluble lignin | 6.8 ± 2.1 | 5.1 ± 0.8 | 2.7 ± 0.3 |
| Cellulose | 44.1 ± 1.1 | 41.7 ± 2.0 | 0.0 |
| Hemicellulose | 18.0 ± 0.6 | 5.2 ± 0.1 | 0.0 |
| Extractives | 4.9 ± 0.4 | - | - |
| Ash | 0.5 ± 0.1 | - | - |
| Others | 12.5 | 6.4 | 3.5 |

*Standard deviation is based on analysis repeated at least three times.

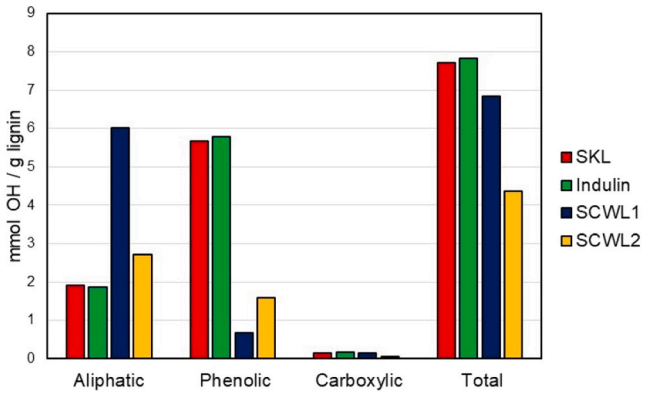


**Fig. 1.** Amount of different OH groups per gram of lignin material obtained by NMR analysis.

*2.3.1. Nuclear magnetic resonance spectroscopy (NMR)*

NMR analysis was conducted on four different lignin samples to further characterize them and gain a deeper understanding of their varying wettability behaviors over time. Sample preparation for NMR followed the protocol outlined by Meng [16]. The analysis was performed using a Bruker Avance Neo (500 MHz, 2 channels) spectrometer (Bremen, Germany) equipped with an i-Probe, located at the Laboratory of Instrumental Techniques (LTI) Research Facilities at the University of Valladolid. The conditions for 31 P[1 H] NMR analysis, using Bruker's zgig sequence (inverse-gated decoupling scheme), included a spectral width of 20000 Hz, a transmitter frequency offset of 140 ppm, acquisition time of 0.8 s, a relaxation time between pulses of 11 s, a pulse width of 90°, and a total number of 128 pulses. All measurements were carried out at a temperature of 25 °C.

*2.3.2. Atomic force microscopy (AFM) – roughness measurement*

The surface roughness of the prepared pellets was measured by the atomic force microscopy technique using the Asylum Research MFP3D BIO (Santa Barbara, California, USA); AFM probe 160AC, OPUS by MikroMasch (Sofia, Bulgaria): AFM mode: AC (tapping mode). Five representative samples were imaged in duplicate. In both replicas, images, and data are taken at three different points around the central area of the samples. The pellets were mounted in standard microscopy slides using epoxy glue. Images of two sizes were acquired at every point: 10×10 μm$^2$ and 1×1 μm$^2$.

*2.3.3. The crystallinity of cellulose in the samples*

X-ray diffraction was used to measure and characterize the crystallinity of the cellulose in the samples on Bruker D8 Discover A25 device, Generator 3Kw, Copper ceramic tube 2.2Kw type FFF, Detector LynxEye 40Kv 30 Ma (Bremen, Germany).

*2.4. Determination of contact angle*

*2.4.1. Measurement of water contact angle*

The contact angle measurements were performed using a High-Pressure View Cell from Eurotechnica GmbH (Bargteheide, Germany) coupled with a high-resolution CCD camera [17]. The internal volume of the cell is 30 ml and the maximum operating conditions are 500 °C and 30 MPa. Measurements were performed using the sessile drop method at a temperature of 25 °C. Nitrogen was used to pressurize the system in the pressure range from atmospheric pressure to 130 bar. The dynamic contact angle was also monitored over approximately 10 min. Mili-Q water was used in all experiments. The contact angle measurements were performed by first placing approximately ten drops of water at the bottom of the cell to saturate the environment (pressurized gas) and minimize the effect of evaporation on the contact angle. The sample was then positioned on the sample holder inside the cell. A single drop was formed at the capillary tip before pressurizing the system to avoid issues with droplet formation under pressure. For experiments conducted at atmospheric pressure, the droplet was placed on the sample immediately after its introduction into the cell. However, when the system was pressurized, the droplet was placed 10–15 minutes after achieving the desired pressure to ensure that the water was saturated with nitrogen and equilibrium between interfacial forces was established. Measurements for all conditions were repeated at least three times, applying a new pellet each time. The frame rate of the video was 10 frames per second. Afterward, individual frames were extracted at specified time intervals by adjusting the recording ratio to 10 (every tenth image was extracted) in a free, open - source VLC media player (VideoLAN, Paris, France). The software Open Drop, released under the GNU GPL open – source license (Free Software Foundation (FSF), Boston, Massachusetts, USA), was used to measure the contact angle between the water and the pellets. All images obtained from the video were used in the analysis.

*2.4.2. Measurement of diiodomethane contact angle*

To determine the SE of all tested materials, additional CA measurements were conducted using the nonpolar compound diiodomethane, following the same sessile drop method under ambient conditions. A 10 μl droplet of diiodomethane was placed on the pellet using a micropipette. The high-resolution CCD camera, as previously described, was used to record the video. Each measurement was repeated twice for accuracy. The Open Drop software was employed to calculate the CA between the diiodomethane and the pellets.

**Table 3**
Surface roughness and initial contact angle of sulfonated kraft lignin (SKL), commercial kraft lignin (Indulin), two supercritical water lignin samples (SCWL), and raw birch wood.

| Sample | Root Mean Square Height (Sq), nm | | Arithmetical Mean Height (Sa), nm | | Initial contact angle |
|---|---|---|---|---|---|
| | 10×10 μm$^2$ | 1×1 μm$^2$ | 10×10 μm$^2$ | 1×1 μm$^2$ | |
| SKL | 75.3 ± 15.1 | 9.8 ± 3.8 | 59.8 ± 12.3 | 7.8 ± 3.1 | 39.9 ° ± 2.2 ° |
| Indulin | 79.6 ± 19.6 | 12.2 ± 6.6 | 59.9 ± 14.5 | 9.7 ± 5.7 | 40.9 ° ± 2.1 ° |
| Raw birch wood | 186.5 ± 54.6 | 6.9 ± 0.7 | 140.3 ± 40.9 | 5.4 ± 0.7 | 63.7 ° ± 5.4 ° |
| SCWL 1 | 55.3 ± 14.3 | 5.4 ± 2.6 | 44.5 ± 11.3 | 4.3 ± 2.2 | 44.4 ° ± 4.1 ° |
| SCWL 2 | 30.9 ± 17.7 | 5.5 ± 1.5 | 22.5 ± 13.0 | 4.2 ± 0.8 | 43.0 ° ± 2.6 ° |

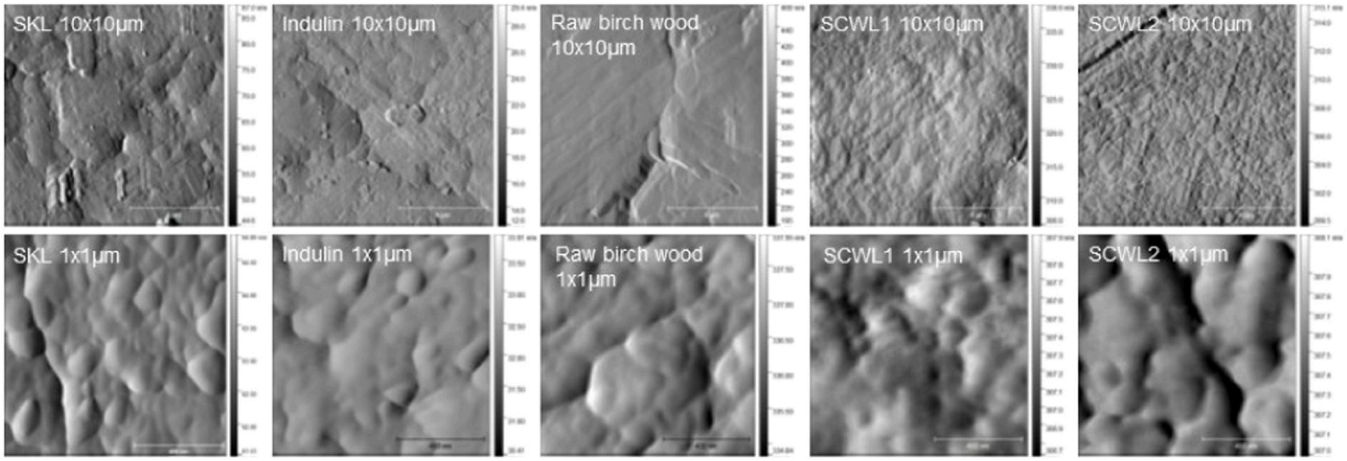


**Fig. 2.** AFM images of tested samples.

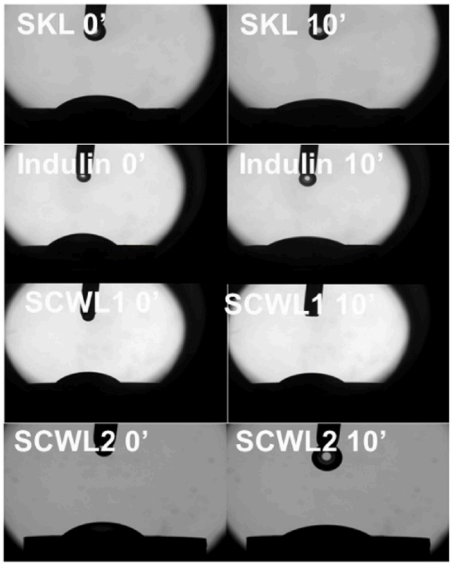


**Fig. 3.** Images of droplet profiles on a solid surface in the first and last minute of recording.

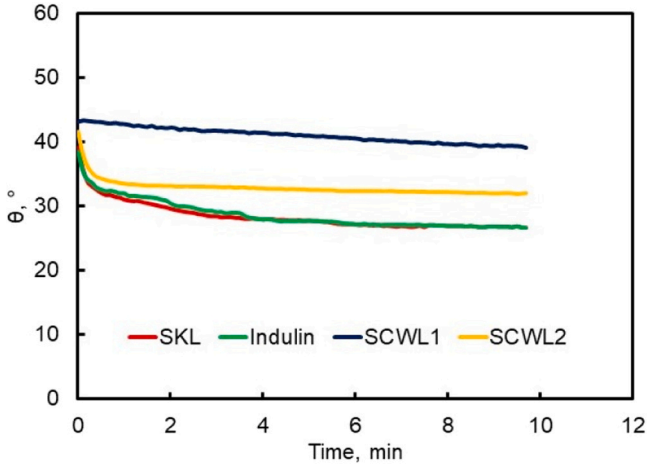


**Fig. 4.** Change of contact angle with time at atmospheric pressure.

**Table 4**
Values of polar and dispersive components and total surface energy for sulfonated kraft lignin (SKL), commercial kraft lignin (Indulin), and two supercritical water lignin samples (SCWL).

| | SKL | Indulin | SCWL1 | SCWL2 |
|---|---|---|---|---|
| SE solid polar, mN/m | 27.2 ± 1.0 | 27.6 ± 2.0 | 21.1 ± 2.4 | 28.2 ± 2.5 |
| SE solid dispers, mN/m | 46.1 ± 0.3 | 45.4 ± 2.3 | 46.6 ± 1.6 | 39.5 ± 2.3 |
| SE solid, mN/m | **73.3** | **73.0** | **67.7** | **67.7** |

*The standard deviation is derived from the standard deviations of the contact angle (CA) measurements, with three replicates for water and two replicates for diiodomethane.

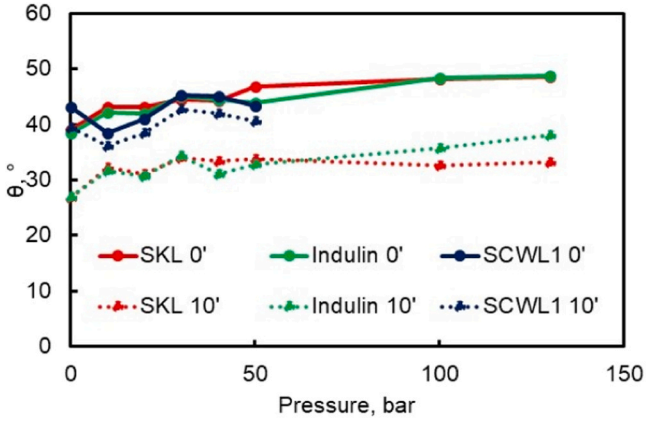


**Fig. 5.** Dependence of initial CA and CA approximately 10 min after droplet deposition on pressure.

### 2.4.3. *Calculation of surface energy - theory*

When a droplet of a liquid is formed on a flat solid surface, the balance on the three-phase interfacial energies is expressed by Young's equation

$$\sigma_s = \sigma_{s,l} + \cos\theta\ \sigma_l \quad (1)$$

where $\sigma_l$ is the surface tension of the liquid, $\theta$ the contact angle between the liquid-air interface and the surface, $\sigma_{s,l}$ is interfacial tension or energy between the solid and the liquid and $\sigma_s$ is the surface energy of the solid. To be able to calculate the surface energy from the contact angle, the unknown variable $\sigma_{s,l}$ must be determined.

Fowkes [18] introduced a concept for dividing the interfacial tension (IFT) or energy into parts of polar and apolar interactions that are added

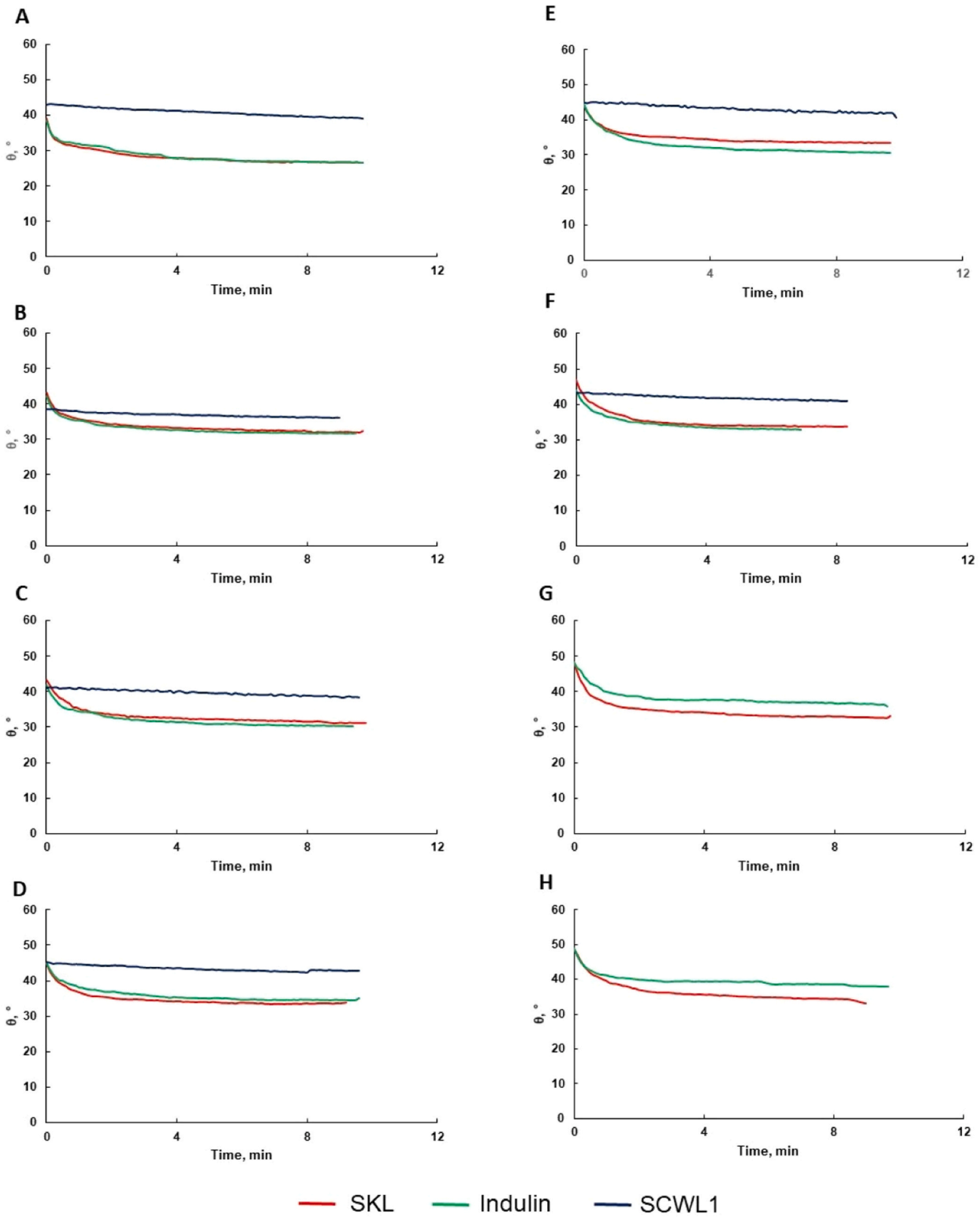


**Fig. 6.** Change of contact angle over time at atmosphere pressure (A), 10 bar (B), 20 bar (C), 30 bar (D), 40 bar (E), 50 bar (F), 100 bar (G), and 130 bar (H).

for obtaining the interfacial tension as a macroscopic measure as shown by Eq. (2)

$$\sigma_s = \sigma_s^d + \sigma_s^p \quad (2)$$

where d means dispersion and p polar component.

According to Fowkes [18], the interfacial tension or energy between two phases, in this case between liquid and solid ($\sigma_{s,l}$), is interpreted as the geometric mean of a polar part and a disperse part

$$\sigma_{s,l} = \sigma_s + \sigma_l - 2\left(\sqrt{\sigma_s^d \sigma_l^d} + \sqrt{\sigma_s^p \sigma_l^p}\right) \quad (3)$$

Combining Eq. (1) and Eq. (3), the following equation is obtained

$$\sigma_l (1 + \cos\theta) = 2\left(\sqrt{\sigma_s^d \sigma_l^d} + \sqrt{\sigma_s^p \sigma_l^p}\right) \quad (4)$$

The surface energy of the solid is determined from the contact angle data in two steps: The disperse part is calculated first with the help of a purely nonpolar liquid. The polar part is then determined with a different liquid with polar parts. The nonpolar liquid is assumed to interact only through disperse interactions with the solid, for which Eq. (4) simplifies to:

$$\sigma_s^d = \sigma_{\text{diiodomethane}} \left(\frac{1+\cos\theta}{2}\right)^2 \quad (5)$$

The dispersive part of the solid surface energy (Eq. (5)) can be used to calculate the corresponding polar part knowing the polar part of the surface tension of a subsequently applied (partly) polar liquid such as water.

$$\sigma_s^p = \frac{1}{\sigma_w^p} \left(\frac{\sigma_w(1+\cos\theta) - 2\sqrt{\sigma_w^d \sigma_s^d}}{2}\right)^2 \quad (6)$$

The surface tension of water at different temperatures is well-known and tabulated [19]. Further, it can be assumed that polytetrafluoroethylene (PTFE) is a completely non-polar solid surface. Then, from Eq. (2), $\sigma_{PTFE}^d = \sigma_{\text{PTFE}}$. The surface energy of PTFE is a very well-known value in the literature [18,20,21]. Consequently, applying these assumptions to Eq. (6) makes it possible to calculate the dispersive part of water surface tension.

$$\sigma_w^d = \frac{\sigma_w^2}{\sigma_{PTFE}} \left(\frac{1+\cos\theta}{2}\right)^2 \quad (7)$$

The polar component of the surface energy is calculated from Eq. (2) as the difference between the surface tension of water and its dispersive component. Using Eqs. 1 through 7, along with literature data for the surface tension of water and diiodomethane [21] under ambient conditions, and the surface energy of PTFE, as well as contact angle values obtained from the previously explained experiments, it is possible to estimate the surface energy of the lignin material. For the SE calculations, the CA values were taken after the system reached mechanical equilibrium.

## 3. Results and discussion

### 3.1. Composition of birch wood and SCWL

The chemical compositions of the birch wood and two SCWL products are given in Table 2. It is evident that the amount of carbohydrates, primarily cellulose, remaining in the product varies based on the hydrolysis conditions. In sample SCWL1, the cellulose content is significant; whereas in SCWL2, it was undetectable by HPLC. As expected, less severe hydrolysis conditions results in a higher cellulose content in the solid product.

### 3.2. Characterization of pellets

#### 3.2.1. Nuclear magnetic resonance spectroscopy (NMR)

NMR analysis (Fig. 1) provided insights into the OH groups content in lignin samples, categorized as aliphatic, phenolic, and carboxylic OH groups. SKL and Indulin showed similar amounts of aliphatic and phenolic OH groups, while, due to its high cellulose content [22], SCWL1 had around 3 times more aliphatic OH groups than Indulin and SKL, and more than double compared to SCWL2. Furthermore, a remarkably higher amount of phenolic OH groups can be observed in SKL and Indulin in comparison to the lignin sample obtained in this work. This phenomenon can be attributed to the unique process by which lignin is obtained using the described method, resulting in a structure that closely retains its native characteristics [13,14]. In this near-native lignin structure, phenolic groups engage in covalent bonding, as evidenced by their distinct signatures observed in NMR analysis. Namely, if the OH group is involved in covalent bonding, such as esterification or etherification, the NMR signals of the OH protons may change or even disappear if the protons are exchanged or if the OH group is no longer free.

#### 3.2.2. Atomic force microscopy (AFM) – roughness measurement

Table 3 presents the surface roughness values of the prepared pellets, while Fig. 2 displays the corresponding AFM images. The surface roughness of raw birch wood pellets (Sq = 186.47 nm; Sa = 140.26 nm) is notably higher compared to the hydrolyzed samples. According to literature, increased surface roughness enhances wetting in water–wet systems, whereas in non-wetted surfaces, it tends to increase the contact angle, a phenomenon known as the lotus effect [23]. Consistent with this, the higher roughness of raw birch wood is associated with a slightly higher initial CA before swelling occurs.

#### 3.2.3. The crystallinity of cellulose in the samples

X-ray diffraction analysis of cellulose crystallinity showed a slight decrease from 61.5 % in raw birch wood to 59.0 % in SCWL1, while SCWL2 showed no detectable crystallinity due to negligible carbohydrate content, as confirmed by HPLC. The transformation of rigid crystalline cellulose into more flexible amorphous structures in SCWH promotes easier hydrolysis, as water molecules avoid hydrophobic zones [12]. Lower crystallinity correlates with higher surface energy, influencing wettability [24].

### 3.3. Contact angle

#### 3.3.1. Change of CA with time

The properties of solid materials are often categorized based on their contact angle (CA). Solids with a CA below 90° are considered hydrophilic, while those with a CA above 90° are classified as hydrophobic [11]. The experimental results demonstrated that all samples were hydrophilic, with CA values consistent with existing literature [25]. Initially, the water droplet profile was monitored at atmospheric pressure over a 10 min period, with the droplet profile shown in Fig. 3 at first and last minute. Despite similar initial CAs, variations in the droplet behavior were observed (Fig. 4). SKL, Indulin, and SCWL2, characterized by a lignin-dominant structure and negligible carbohydrates, exhibited significant CA changes within the first 60 seconds. In contrast, SCWL1, with a higher cellulose content, displayed a more linear droplet profile. These behaviors can be attributed to different mechanisms such as absorption, spreading, swelling, and evaporation [10]. Absorption and spreading were dominant in the first minute, while evaporation was negligible due to the controlled environment (22–25°C). The swelling was observed exclusively in the raw birch wood, which is presumably attributed to its high cellulose content (44.1 %). This phenomenon has been previously reported in cellulose crystallites [26,27]. In SCWL1, the increased lignin content (46.7 %) likely restricted swelling by reducing cellulose exposure to water through hydrogen bonding between

cellulose and lignin. Then, the availability of the free OH groups to interact with water is reduced [28].

### 3.3.2. Surface energy

Surface energy estimates for the tested materials (Table 4) indicated that materials with higher surface energy exhibit better wettability [29]. SKL and Indulin, which had the same wettability behavior (Fig. 4), also had comparable surface energies. Furthermore, their polar and dispersive components were analogous. On the other hand, the SE of SCWL1 and SCWL2 were slightly lower than SKL and Indulin. Notably, SCWL1 exhibited a dispersive component similar to SKL and Indulin, but with a lower polar component due to its high cellulose content, which contributes to the dispersive SE. Despite their polar nature, carbohydrates also possess a dispersive component of surface energy due to the presence of non-polar carbon-hydrogen bonds and ring structures. As such, it contributes to the dispersive part of the surface energy of the SCWL1 sample. Additionally, it can be concluded that a relatively high crystallinity of cellulose presented in this sample (59 %) contributes to the lower surface energy, particularly, its polar component. In contrast, the polar component of SCWL2 is comparable to the polar parts of SKL and Indulin, while the dispersive component was significantly lower. It is known that the dispersive component of the surface energy in lignin is attributed to van der Waals forces arising from the non-polar interactions between the aromatic rings and carbon-hydrogen bonds. Although lignin has polar groups, its aromatic nature promotes a significant dispersive component [18,30]. The method of extraction significantly affects properties like wettability and SE [31], with the molecular weight of lignin influencing dispersive SE through chain mobility, surface roughness, intermolecular interactions, surface composition, solubility, and thermodynamic stability. Commercial lignins, like SKL and Indulin, typically have lower molecular weight, resulting in higher surface energy due to increased molecular mobility and interaction potential, while higher molecular weight lignins tend to have lower surface energy due to reduced mobility and more extensive intermolecular interactions [32]. In contrast, SCWH allows for precise control of conditions, producing lignin with higher molecular weight and closer to its native structure [13,14], which contributes to its lower dispersive SE.

Finally, this study highlights the advantage of using SCWH to obtain lignin and lignin-cellulose composites. By fine-tuning reaction conditions, SCWH allows selective fractionation of biomass components while preserving lignin's structure and controlling the cellulose content in the final product. The biomass components can be selectively targeted and efficiently separated, optimizing the yield of desired products. In this process, when lignocellulose biomass is hydrolyzed to obtain lignin, it is possible not only to keep its structure closer to native, but also is feasible to control the amount of cellulose remaining in the product. As a result, the wettability of these materials can be tailored for optimal performance in composite manufacturing.

### 3.3.3. Dependence of CA on pressure

Fig. 5 shows the variation in initial CA and CA approximately 10 minutes after droplet deposition, as a function of pressure for three tested samples: SKL, Indulin, and SCWL1. In all cases, a slight increase in CA is observed with increasing pressure. According to Young's relation and considering the decreasing interfacial tension (IFT) with pressure [17], the surface energy at the solid-gas interface decreases as the pressure rises. These findings are consistent with results reported by Song and Fan [33]. Lastly, Fig. 6 shows that the overall dynamic behavior of the SKL, Indulin, and SCWL1 surfaces remains largely unaffected by changes in pressure.

## 4. Conclusions

In this work, the wettability properties of lignin-cellulose composites were characterized and compared to lignins from different origins and extraction methods, such as SKL or Indulin. The hydrophilicity of all tested samples was confirmed, with contact angles (CA) consistent with literature values. Observations of water droplet profile evolution over time revealed differences, primarily driven by absorption and spreading during the initial stage after droplet formation. Raw birch wood, with its high carbohydrate content, exhibited swelling. X-ray diffraction analysis showed a slight reduction in cellulose crystallinity in SCWL1 after the process of SCWH, whereas the crystallinity was undetected in SCWL2 due to its low carbohydrate content. Materials with higher surface energy exhibited enhanced wettability. SKL and Indulin displayed similar surface energy and wettability behavior, while SCWL1 and SCWL2 presented slightly lower surface energies and higher CAs. Differences in the polar and dispersive components were attributed to varying cellulose and lignin contents. Nuclear magnetic resonance analysis revealed substantial differences in aliphatic and phenolic hydroxyl group content among samples, with SCWH-obtained lignin showing covalent bonding that influenced NMR visibility. These findings elucidate the significant impact of material composition and processing on wettability and surface energy. Therefore, when applied to lignocellulose biomass like birch wood, SCWH not only preserves the lignin's structure close to its native form but also enables control of cellulose content in the final product, allowing for tailored wettability and optimal properties for composite preparation.

## CRediT authorship contribution statement

**Philip Jaeger:** Writing – review & editing, Validation, Formal analysis, Data curation, Conceptualization. **Vesna Leontijevic:** Writing – original draft, Methodology, Investigation. **Maria Jose Cocero:** Writing – review & editing, Supervision, Resources, Project administration, Investigation, Funding acquisition, Formal analysis, Conceptualization. **Danilo Cantero:** Writing – review & editing, Supervision, Formal analysis. **Tijana Fechter:** Methodology, Formal analysis, Conceptualization.

## Declaration of Competing Interest

The authors declare that they have no known competing financial interests or personal relationships that could have appeared to influence the work reported in this paper.

## Acknowledgments

This work was supported by the Agencia Estatal de Investigación (Gobierno de España) and FEDER Funds PID2022–140930NB-I00 and TED2021–129837B-C42; and Junta de Castilla y León - Consejería de Educación and FEDER Funds [CLU-2019–04]. V Leontigevic thanks JCyL for his predoctoral contract. D. Cantero is funded by the Spanish Ministry of Science, Innovation and Universities (Beatriz Galindo fellowship BEAGAL18/00247).

## Data Availability

Data will be made available on request.

## References

[1] N. Abad-Fernández, E. Pérez, M.J. Cocero, Aromatics from lignin through ultrafast reactions in water, Green. Chem. 21 (2019) 1351–1360, https://doi.org/10.1039/c8gc03989e.

[2] S. Zhang, X. Meng, S. Bhagia, A. Ji, M. Dean Smith, Y. Wang, B. Liu, C.G. Yoo, D. P. Harper, A.J. Ragauskas, 3D printed lignin/polymer composite with enhanced mechanical and anti-thermal-aging performance, Chem. Eng. J. 481 (2024) 148449, https://doi.org/10.1016/j.cej.2023.148449.

[3] M.Y. Balakshin, E.A. Capanema, I. Sulaeva, P. Schlee, Z. Huang, M. Feng, M. Borghei, O.J. Rojas, A. Potthast, T. Rosenau, New opportunities in the valorization of technical lignins, ChemSusChem 14 (2021) 1016–1036, https://doi.org/10.1002/cssc.202002553.

[4] H. Punia, J. Tokas, S. Bhadu, A. Rani, S. Sangwan, A. Kamboj, S. Yashveer, S. Baloda, Nanocellulose as reinforcement materials for polymer matrix composites. Handb. Nanocelluloses, Springer International Publishing, Cham, 2022, pp. 407–440, https://doi.org/10.1007/978-3-030-89621-8_25.
[5] M.Ö. Seydibeyoğlu, A. Dogru, J. Wang, M. Rencheck, Y. Han, L. Wang, E. A. Seydibeyoğlu, X. Zhao, K. Ong, J.A. Shatkin, S. Shams Es-haghi, S. Bhandari, S. Ozcan, D.J. Gardner, Review on hybrid reinforced polymer matrix composites with nanocellulose, nanomaterials, and other fibers, Polym. (Basel) 15 (2023) 984, https://doi.org/10.3390/polym15040984.
[6] V. Khoshkava, M.R. Kamal, Effect of surface energy on dispersion and mechanical properties of polymer/nanocrystalline cellulose nanocomposites, Biomacromolecules 14 (2013) 3155–3163, https://doi.org/10.1021/bm400784j.
[7] M.R. Kamal, J.U. Calderon, B.R. Lennox, Surface energy of modified nanoclays and its effect on polymer/clay nanocomposites, J. Adhes. Sci. Technol. 23 (2009) 663–688, https://doi.org/10.1163/156856108X379164.
[8] D.Y. Kwok, A.W. Neumann, Contact angle interpretation in terms of solid surface tension, Colloids Surf. A Physicochem. Eng. Asp. 161 (2000) 31–48, https://doi.org/10.1016/S0927-7757(99)00323-4.
[9] D. Ahmad, I. van den Boogaert, J. Miller, R. Presswell, H. Jouhara, Hydrophilic and hydrophobic materials and their applications, Energy Sources, Part A Recover. Util. Environ. Eff. 40 (2018) 2686–2725, https://doi.org/10.1080/15567036.2018.1511642.
[10] S. Farris, L. Introzzi, P. Biagioni, T. Holz, A. Schiraldi, L. Piergiovanni, Wetting of biopolymer coatings: contact angle kinetics and image analysis investigation, Langmuir 27 (2011) 7563–7574, https://doi.org/10.1021/la2017006.
[11] T. Zhao, L. Jiang, Contact angle measurement of natural materials, Colloids Surf. B Biointerfaces 161 (2018) 324–330, https://doi.org/10.1016/j.colsurfb.2017.10.056.
[12] M.J. Cocero, Á. Cabeza, N. Abad, T. Adamovic, L. Vaquerizo, C.M. Martínez, M. V. Pazo-Cepeda, Understanding biomass fractionation in subcritical & supercritical water, J. Supercrit. Fluids 133 (2018) 550–565, https://doi.org/10.1016/j.supflu.2017.08.012.
[13] T. Adamovic, D. Tarasov, E. Demirkaya, M. Balakshin, M.J. Cocero, A feasibility study on green biorefinery of high lignin content agro-food industry waste through supercritical water treatment, J. Clean. Prod. 323 (2021) 129110, https://doi.org/10.1016/j.jclepro.2021.129110.
[14] D. Rigo, T. Fechter, E. Capanema, D. Diment, M. Alopaeus, D. Tarasov, D. Cantero, M. Balakshin, Isolation of β–O–4-rich lignin from Birch in high yields enabled by continuous flow supercritical water treatment, ChemSusChem (2024), https://doi.org/10.1002/cssc.202401683.
[15] A. Sluiter, B. Hames, R. Ruiz, C. Scarlata, J. Sluiter, D. Templeton, D. Crocker, Determination of structural carbohydrates and lignin in biomass, Natl. Renew. Energy Lab 17 (2008) https://doi.org/NREL/TP-510-42618.NREL.
[16] X. Meng, C. Crestini, H. Ben, N. Hao, Y. Pu, A.J. Ragauskas, D.S. Argyropoulos, Determination of hydroxyl groups in biorefinery resources via quantitative 31P NMR spectroscopy, Nat. Protoc. 14 (2019) 2627–2647, https://doi.org/10.1038/s41596-019-0191-1.
[17] T. Fechter, R. Villablanca, V. Leontijevic, A. Martin, P. Jaeger, M.J. Cocero, Interfacial tension of water near to critical conditions by using the pendant drop method: New experimental data and a correlation based on the parachor method, J. Supercrit. Fluids 196 (2023) 105899, https://doi.org/10.1016/j.supflu.2023.105899.
[18] F.M. Fowkes, Attractive forces at interfaces, Ind. Eng. Chem. 56 (1964) 40–52, https://doi.org/10.1021/ie50660a008.
[19] S. Cantin, M. Bouteau, F. Benhabib, F. Perrot, Surface free energy evaluation of well-ordered Langmuir-Blodgett surfaces: comparison of different approaches, Colloids Surf. A Physicochem. Eng. Asp. 276 (2006) 107–115, https://doi.org/10.1016/j.colsurfa.2005.10.025.
[20] E.I. Vargha-Butler, H.A. Hamza, A.W. Neumann, Surface tension effects in the sedimentation of polymer particles in various liquid mixtures, J. Dispers. Sci. Technol. 6 (1985) 357–379, https://doi.org/10.1080/01932698508943958.
[21] A. Zdziennicka, J. Krawczyk, K. Szymczyk, B. Jańczuk, Components and parameters of liquids and some polymers surface tension at different temperature, Colloids Surf. A Physicochem. Eng. Asp. 529 (2017) 864–875, https://doi.org/10.1016/j.colsurfa.2017.07.002.
[22] H. Ben, X. Chen, G. Han, Y. Shao, W. Jiang, Y. Pu, A.J. Ragauskas, Characterization of whole biomasses in pyridine based ionic liquid at low temperature by 31P NMR: an approach to quantitatively measure hydroxyl groups in biomass as their original structures, Front. Energy Res. 6 (2018) 1–7, https://doi.org/10.3389/fenrg.2018.00013.
[23] M. Zhang, S. Feng, L. Wang, Y. Zheng, Lotus effect in wetting and self-cleaning, Biotribology 5 (2016) 31–43, https://doi.org/10.1016/j.biotri.2015.08.002.
[24] H. El Omari, E. Ablouh, F. Brouillette, M. Taourirte, A. Belfkira, New method for determining paper surface energy per contact angle, Cellulose 26 (2019) 9295–9309, https://doi.org/10.1007/s10570-019-02695-4.
[25] S. Rodríguez-Fabià, J. Torstensen, L. Johansson, K. Syverud, Hydrophobisation of lignocellulosic materials part I: physical modification, Cellulose 29 (2022) 5375–5393, https://doi.org/10.1007/s10570-022-04620-8.
[26] L.K. Tolonen, P.A. Penttilä, R. Serimaa, A. Kruse, H. Sixta, The swelling and dissolution of cellulose crystallites in subcritical and supercritical water, Cellulose 20 (2013) 2731–2744, https://doi.org/10.1007/s10570-013-0072-7.
[27] S. Rbihi, A. Aboulouard, L. Laallam, A. Jouaiti, Contact angle measurements of cellulose based thin film composites: wettability, surface free energy and surface hardness, Surf. Interfaces 21 (2020) 100708, https://doi.org/10.1016/j.surfin.2020.100708.
[28] K. Łupina, D. Kowalczyk, M. Lis, A. Raszkowska-Kaczor, E. Drozłowska, Controlled release of water-soluble astaxanthin from carboxymethyl cellulose/gelatin and octenyl succinic anhydride starch/gelatin blend films, Food Hydrocoll. 123 (2022) 107179, https://doi.org/10.1016/j.foodhyd.2021.107179.
[29] H. Zhang, J. Xie, S. An, X. Qian, H. Cheng, F. Zhang, X. Li, A novel measurement of contact angle on cylinder-shaped lignocellulosic fiber for surface wettability evaluation, Colloids Surf. A Physicochem. Eng. Asp. 540 (2018) 106–111, https://doi.org/10.1016/j.colsurfa.2017.12.054.
[30] C.J. van Oss, R.J. Good, M.K. Chaudhury, Additive and nonadditive surface tension components and the interpretation of contact angles, Langmuir 4 (1988) 884–891, https://doi.org/10.1021/la00082a018.
[31] M.A. Karaaslan, M.J. Cho, L.Y. Liu, H. Wang, S. Renneckar, Refining the properties of softwood kraft lignin with acetone: effect of solvent fractionation on the thermomechanical behavior of electrospun fibers, ACS Sustain. Chem. Eng. 9 (2021) 458–470, https://doi.org/10.1021/acssuschemeng.0c07634.
[32] D.A. Baker, T.G. Rials, Recent advances in low-cost carbon fiber manufacture from lignin, J. Appl. Polym. Sci. 130 (2013) 713–728, https://doi.org/10.1002/app.39273.
[33] J.W. Song, L.W. Fan, Understanding the effects of pressure on the contact angle of water on a silicon surface in nitrogen gas environment: contrasts between low- and high-temperature regimes, J. Colloid Interface Sci. 607 (2022) 1571–1579, https://doi.org/10.1016/j.jcis.2021.09.021.